International Journal of Fatigue 156 (2022) 106643

Contents lists available at ScienceDirect

International Journal of Fatigue

journal homepage: www.elsevier.com/locate/ijfatigue

Fatigue resistance evaluation of high Mn-TWIP steel through damage mechanics: A new method based on stiffness evolution

Sergi Parareda [a,c,*], Daniel Casellas [a,b], Antoni Lara [a], Antonio Mateo [c]

[a] Eurecat, Centre Tecnològic de Catalunya, Unit of Metallic and Ceramic Materials, 08243 Manresa, Spain
[b] Luleå University of Technology, Division of Mechanics of Solid Materials, 971 87 Luleå, Sweden
[c] CIEFMA – Department of Materials Science and Metallurgical Engineering, EEBE, Universitat Politècnica de Catalunya-BarcelonaTech, 08019 Barcelona, Spain

ARTICLE INFO

Keywords:
Fatigue test methods
Damage mechanics
Fatigue limit
Fatigue crack growth
Steels

ABSTRACT

The work presented here deals with the implementation of a new methodology that allows fast and reliable determination of the fatigue strength. It is based on monitoring the specimen stiffness changes at different stress levels, as an indicator of the evolution of fatigue damage. This new rapid fatigue test uses techniques available in many laboratories, as the DIC (Digital Image Correlation) technique and common extensometers. Moreover, the obtained data are easier to handle than infrared cameras or acoustic emission systems data, and the experimental procedure to determine the fatigue limit is more evident than in the self-heating method.

Experiments have been conducted in TWIP (Twinning Induced Plasticity) steel, a material used for light-weighting the structural parts of vehicles. With their excellent energy absorption capacity, TWIP steels can satisfy the part requirements in terms of crash performance, while their high tensile strength can deal with the cyclic loads acting on chassis parts. Therefore, many efforts focus on improving the fatigue strength of TWIP steels through pre-straining and/or surface treatments. However, finding the best way to improve the fatigue resistance requires time and resources that often hinder the development of the material. For this reason, a TWIP steel has been selected to check the new rapid fatigue test. The prediction made using the proposed approach is validated by comparison with conventional staircase results and fatigue crack growth standardised tests. The good agreement allows proposing the new method as a fast and efficient way to determine the fatigue resistance in metals.

1. Introduction

High manganese austenitic steels (HMnS) show an outstanding combination of formability and strength, thanks to the twinning-induced plasticity (TWIP) effect, that poses them as good candidates for vehicle lightweighting [1–4]. They are also known as TWIP steels and belong to the 2nd generation of Advanced High Strength Steels (AHSS). Their superior mechanical performance is related to the value of the stacking fault energy (SFE), mainly controlled by the chemical composition [5,6] and temperature [7]. TWIP effect is reported for SFE values from 20 to 60 mJ/m^2 [8]. Alloying elements generally decrease the SFE, leading to an enhanced twinning behaviour during deformation. Nonetheless, a SFE below 20 mJ/m^2 favours the austenite (γ_{fcc}) to martensite (ε_{hcp}, α'_{bcc}) transformation, known as the transformation-induced plasticity (TRIP) effect [9,10]. This effect is suppressed by the addition of Al that increases the SFE and promotes the mechanical twinning formation [11]. Twinning conducts a superior strain hardening capability that may be understood as a dynamic Hall-Petch effect [12]. Such phenomenon confers to TWIP steels a high fracture toughness, which enables them for the production of crash-resistant parts of the body in white (BiW) [13–15]. TWIP steels could also be applied to other parts of the vehicles as suspension arms or chassis parts [16]. However, these parts are subjected to cyclic loads during vehicle use, which means that their fatigue resistance must be known.

Since the first fatigue evaluation of TWIP steels reported by Cornette et al. [17], several authors have studied their fatigue behaviour, reporting different fatigue limit values as a function of the applied stress ratio R (σ_e) [18]. Fatigue limits of about 400 MPa were measured for R = -1 [19,20] and 260 MPa for R = 0.1 [21], both expressed in terms of stress amplitude. The fatigue limit for R = 0.1 to ultimate tensile strength (σ_e / σ_{UTS}) ratio is around 0.2 [22]. This ratio is lower for TWIP steels than the ones obtained for other AHSS of similar strength, such as

* Corresponding author at: Eurecat, Centre Tecnològic de Catalunya, Unit of Metallic and Ceramic Materials, 08243 Manresa, Spain.
E-mail address: sergi.parareda@eurecat.org (S. Parareda).

https://doi.org/10.1016/j.ijfatigue.2021.106643
Received 2 August 2021; Received in revised form 22 October 2021; Accepted 7 November 2021
Available online 20 November 2021

Table 1
Chemical composition of the investigated TWIP steel in weight percentage.

Fe	C	Mn	Si	Al	Ti	N	S	Others
Bal.	0.35	19.90	0.20	1.00	0.006	0.013	0.0003	Cr, Ni, Cu, V

complex-phase (CP) and dual-phase (DP) steels, that show σ_e / σ_{UTS} values larger than 0.25 [23,24]. Such ratio for TWIP steels is similar to the one found for austenitic stainless steels or press hardening steels (PHS) [25,26].

Such a low σ_e / σ_{UTS} ratio for TWIP steels has stimulated the research to improve their high cycle fatigue (HCF) resistance. Most of the works focused on pre-straining strategies [27–33], grain refinement [34,35], alloy optimisation [36–38] or surface treatments [39–41]. It is accepted that the general enhancement of the HCF resistance comes from the presence of twins induced by pre-straining the material [28]. However, the consequent improvement in tensile strength also increases the notch sensitivity, promoting crack initiation at inclusions or surface defects, which lowers the σ_e / σ_{UTS} ratio [29]. For this reason, more research on the HCF resistance is needed to deeply understand the relationship between the microstructural characteristics of TWIP steels and their fatigue resistance.

However, it should be kept in mind that HCF tests are expensive and time-consuming, which limits the generation of data for different material and processing conditions. So, accelerated or more straightforward testing procedures would help to further progress in microstructural development of fatigue optimised steel grades. One of the first fatigue test methods to rapidly determine the fatigue limit was proposed by Stromeyer [42]. Other authors further developed this method by using thermography [43–46]. The method is based on measuring the self-heating effects during fatigue testing, associated with the dissipated thermal energy. The procedure has been applied to determine the fatigue limit of austenitic stainless steels [47,48] and TRIP steels [49]. Nevertheless, Meneghetti [50] reported that the method is unsuitable for all types of metals and testing facilities.

This work aims to use rapid fatigue tests to evaluate the fatigue resistance of TWIP steels. A novel rapid fatigue test, based on continuum damage mechanics (CDM), is proposed to overcome the drawbacks shown by the self-heating method. According to the CDM theory, the test gives a damage variable through the measurement of the stiffness evolution [51,52]. In this way, the fatigue damage evolution is easily monitored from the undamaged material to the macroscopic crack initiation, as shown by finite element methods based on CDM [53–55]. Moreover, the proposed test also allows to measure the propagation of large cracks and rationalize it following fracture mechanics concepts. TWIP steels show excellent resistance to fatigue crack propagation with a large stable crack propagation regime [56]. This behaviour is perfect to check the applicability of the method to catch the two main stages of fatigue damage: crack initiation and propagation.

2. Material and experimental procedure

2.1. Material

This work investigates a fully austenitic TWIP steel, supplied as cold-rolled sheets of 1.45 mm in thickness. The chemical composition obtained by spark atomic emission spectrometry is summarised in Table 1. Tensile properties were determined at room temperature using a universal testing machine according to the ISO 6892 standard, in longitudinal and transverse orientations concerning the sheet rolling direction (RD). The fracture toughness was evaluated through elastic-plastic fracture mechanics measurements following the essential work of fracture methodology, adapted to AHSS by Frómeta et al. [13].

The microstructure is austenitic, as expected for the Mn-Al-Si alloyed steel [57]. Fig. 1 shows etched images, longitudinal and transverse to RD, analysed by Field Emission Scanning Electron Microscopy (FE-

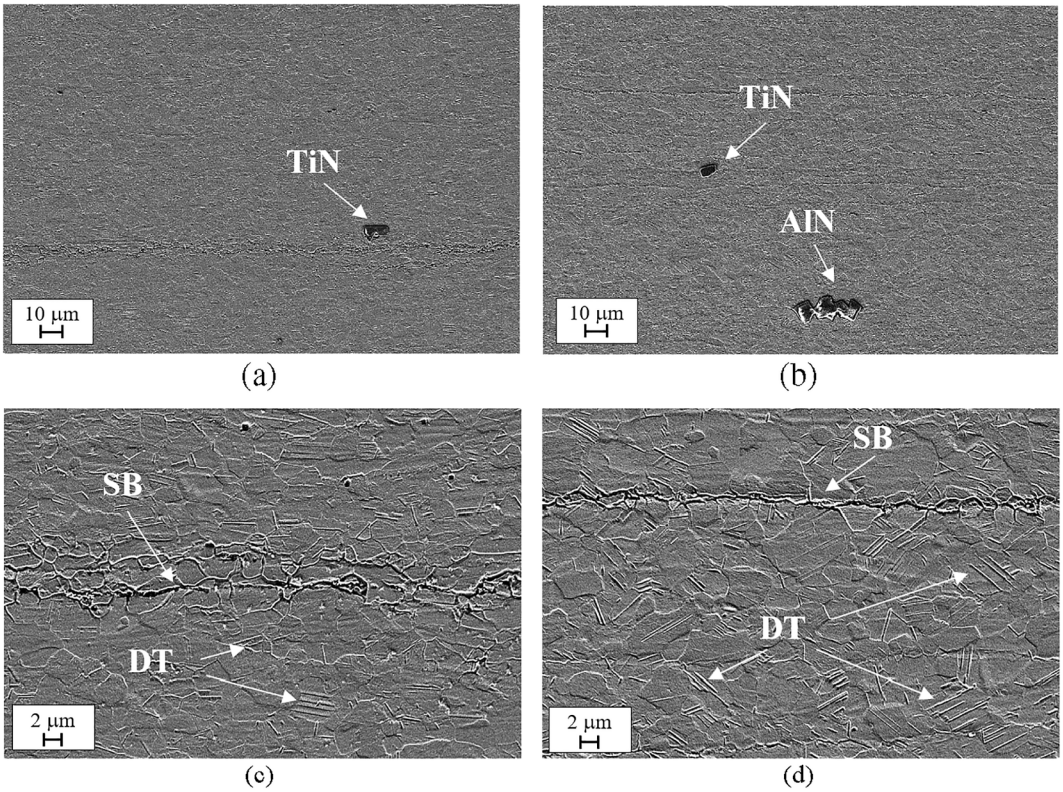

Fig. 1. Microstructure of the studied TWIP steel: (a) longitudinal and (b) transverse to RD with indicated TiN and AlN non-metallic inclusions; deformation twins (DT) and shear bands (SB) are indicated as well in (c) longitudinal and (d) transverse to RD images.

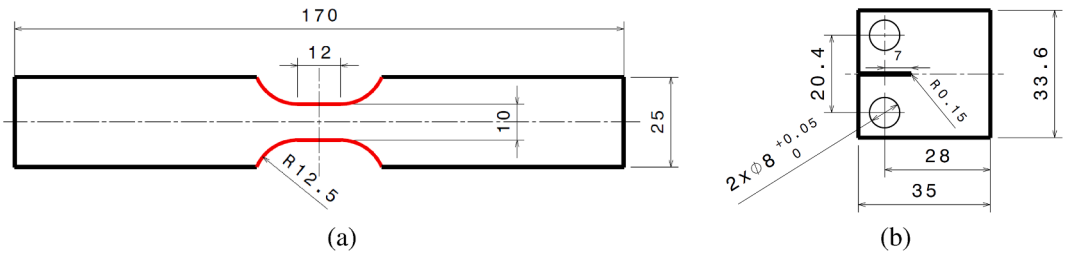

Fig. 2. a) Uniform gauge (SEN(T)) fatigue specimen ($K_f = 1.12$) with the polished edge (in red colour). b) Dimensions of C(T) specimen for thin sheets according to ASTM E647 used in the present work. Dimensions are expressed in mm.

SEM). These images were used to measure the mean grain size following the linear intercept method. The grain size is 4.6 ± 1.2 μm. The observed non-metallic inclusions were identified by an Energy Dispersive X-ray Spectrometry analyser (EDX). Most of them are AlN, together with some typical cubic shaped TiN particles. Elongated AlN inclusions along the rolling direction can act as fatigue crack initiation sites, as reported by several authors [58,59]. Deformation twins (DT) and shear bands (SB) induced by the cold-rolling process can be discerned, similar to those reported by Kusakin [60].

2.2. Fatigue tests

The fatigue limit (σ_e) was evaluated by three different tests: the conventional staircase or up-and-down method, the rapid fatigue test based on self-heating measurements and the rapid fatigue test based on stiffness evolution. The latter is a novel method based on fatigue damage, and it is described in detail in section 3.

The fatigue tests were performed using the uniform gauge specimens shown in Fig. 2a, named as SEN(T) by their similarity to the single edge notch tension specimens once a crack appears. The specimen geometry was the same as used by the authors in a previous work to investigate the low cycle fatigue resistance of the present TWIP steel [41]. The specimens were machined by spark erosion in the transverse direction concerning the RD and edge polished to specular finish. The surface roughness was measured with an optical 3D measurement system, giving a R_a value of 1.6 ± 0.2 μm (typical surface finish for cold rolled blanks). The specimens were tested at room temperature in a servo-hydraulic testing machine MTS 322 Test Frame, using a stress ratio ($R = \sigma_{min} / \sigma_{max}$) of 0.1 and a frequency of 30 Hz.

2.2.1. Conventional fatigue test

In the staircase method [61], the σ_e was determined as the fatigue strength corresponding to 2 million cycles. Tests were carried out following the ASTM E466 standard [62]. At least 15 specimens were tested and the obtained value of σ_e is used to validate the results obtained with the rapid methods.

2.2.2. Rapid fatigue test based on self-heating measurements

The σ_e was measured through the self-heating method following the descriptions given in [43]. The method is based on monitoring the temperature of the specimen while cyclically loaded with increasing stress amplitude blocks. The measured increase of temperature is related to the dissipation of micro-deformation energy induced by the fatigue blocks. Once the specimen breaks the mean steady temperature of each fatigue block is plotted against the applied stress amplitude. The fatigue limit is then determined as the intersection between the first and second regimes, described and shown in Fig. 4b. Tests were performed with the same successive blocks of cyclic loadings, further described for the stiffness method. The mean steady-state temperature was evaluated by each fatigue block through an infrared camera FLIR systems A655sc, resolution: 640 × 480 pixels and spectral range 7.5–14 μm. Specimens were painted with a high emissivity black paint (emissivity of 0.96) and enclosed in an insulating chamber during the test to avoid heat reflections of external sources. An unloaded, black-painted aluminium plate was located inside the chamber and used as a black body to monitor the environmental temperature.

2.2.3. Fatigue crack growth resistance

Aimed at relating the measured σ_e with initial defects and with intrinsic material crack propagation resistance, fatigue crack growth rate (FCGR) test was performed according to the ASTM E647 procedure [63]. Small compact tension C(T) specimens were machined by spark erosion in the longitudinal direction concerning the RD, i.e. in the T-L direction according to ASTM E1823 notation [64]. The geometrical dimensions of the specimen are shown in Fig. 2b. The test was conducted at room temperature and a frequency of 60 Hz on a resonance fatigue testing machine (RUMUL Testronic) under an R of 0.1. The crack length was measured using crack growth gauges glued at both sides of the specimen. After pre-cracking at a constant $\Delta K = 12$ MPa $m^{1/2}$, the software was programmed for decreasing ΔK until the ΔK_{TH} was reached. The ΔK_{TH} was defined as the value of ΔK with a crack propagation velocity lower than 10^{-11} m / cycle. Finally, the test was stopped and started again in constant increasing ΔK mode until the failure of the specimen. Crack propagation rate results, da / dN, were described by the Paris-Erdogan law

$$\frac{da}{dN} = C(\Delta K)^m \tag{1}$$

where a is the crack length, N the number of cycles and C and m are the Paris coefficients. Following Linear Elastic Fracture Mechanics (LEFM) concepts ΔK is defined as

$$\Delta K = Y \Delta\sigma \sqrt{\pi a} \tag{2}$$

where Y is a dimensionless factor related to crack geometry and $\Delta\sigma$ is the applied stress range. Paris coefficients, C and m, were obtained from experimental data fitting to Eq. (1).

3. Rapid fatigue test based on stiffness evolution

CDM defines fatigue damage as a gradual deterioration of the structure of a material caused by the accumulation and growth of micro and macro cracks [65]. The stress level at which such damage evolves into fatigue propagating cracks defines the σ_e of the material. Following this statement, the rapid fatigue testing method presented in this work suggests estimating σ_e by monitoring the damage developed during cyclic testing.

Following the CDM concepts, damage can be represented by the damage variable (D), defined for uniaxial specimens as

$$1 - D = \frac{\widetilde{A}}{A} \tag{3}$$

where A is the net area of the specimen in the undamaged state ($D = 0$), and $\widetilde{A}$ is the residual area because of the formation of microcracks ($0 \leq D \leq 1$). Such area ratio gives the reduction of the effective area to bear a

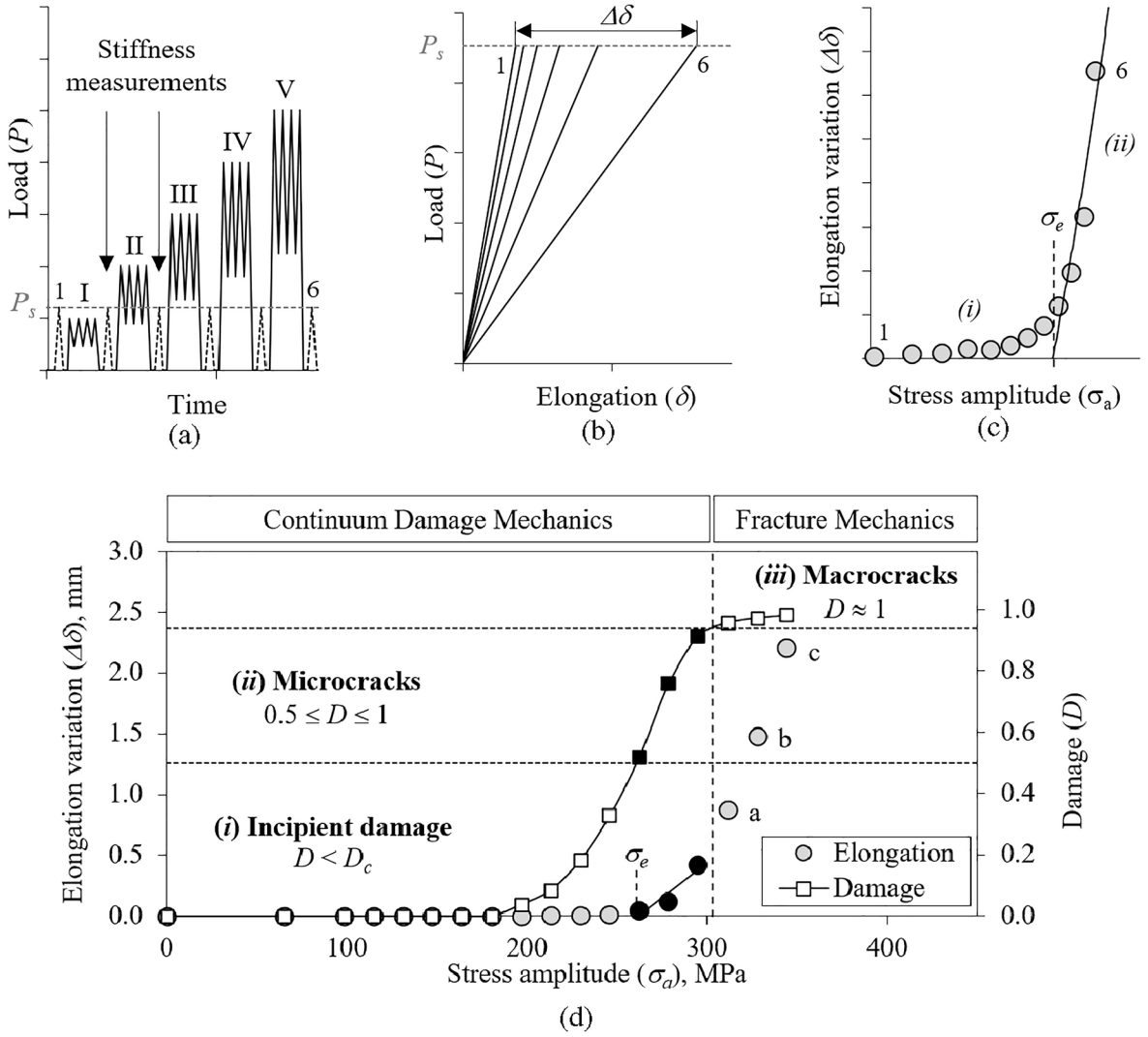

Fig. 3. Schematic representation for a) successive series of cyclic loads with increasing stress amplitude and elongation measurements, b) stiffness reduction throughout the test, c) elongation curve to determine the fatigue limit and d) elongation variation and damage evolution for the investigated TWIP steel showing the two different regimes (*i*, *ii*) related to CDM and the regime (*iii*) where fracture mechanics explains crack growing. The points labelled as a, b and c are used in Fig. 6.

given load. It is directly related to the elastic behaviour of the material because as the microcracks grow, the stiffness decreases and consequently, the compliance increases (Fig. 3b). Thus, the damage may be estimated by measuring the elastic response of the material for the undamaged (E) and damaged ($\tilde{E}$) state according to

$$1 - D = \frac{1}{E}\frac{d\sigma}{d\varepsilon} = \frac{\tilde{E}}{E} \tag{4}$$

The Eq. (4) can be rearranged to facilitate the experimental measurements. Considering 0.1 mm^3 as the Representative Volume Element (RVE) for metals, it is assumed that the nominal stress is maintained and that the change in the stiffness is given by the strain variation [66]. Hence, the engineering strain (e and $\tilde{e}$) or the elongation (δ and $\tilde{\delta}$) at a fixed load level (P_S) can be used to determine the damage as

$$D = 1 - \frac{\tilde{E}}{E} \; 1 - \frac{e}{\tilde{e}} = 1 - \frac{\delta}{\tilde{\delta}} \tag{5}$$

Hence, the method proposes evaluating σ_e from the evolution of the fatigue damage by monitoring the specimen stiffness at different stress levels. According to this experimental approach, the method (under patent EP20382742.3) is named as the *stiffness method* from now on.

A complete test consists of the application of successive blocks of cyclic loads, progressively increasing the stress amplitude (σ_a) and measuring the stiffness after each block (Fig. 3a). The elongation (δ and $\tilde{\delta}$) is measured with a Digital Image Correlation (DIC) system, a GOM Aramis SRX equipment in this work. The gauge length to measure the change in stiffness should be large enough to include the damaged zone of the specimen and can be measured with any common extensometer. In this work, it was set at 25 mm. The size of the fatigue blocks was 6000 cycles, with an increasing amplitude (d) of 35 MPa between each other and the P_S for the stiffness determination was set at 4000 N (or nominal stress of 275 MPa). The increment d is determined following the approach used for the staircase method [61]. The test ends when the specimen breaks. The different values of elongation change ($\Delta\delta$) represented in Fig. 3b are plotted against the stress amplitude or maximum stress (σ_{max}) of the previous fatigue block (Fig. 3c). The resulting plot gives the evolution of stiffness variation at different stress levels, from undamaged states ($D = 0$) to final specimen fracture ($D = 1$).

The points from the elongation curve used to estimate the σ_e are defined based on the damage concepts. CDM defines the critical damage level (D_c) as the level at which the incipient damage evolves into

Table 2
Monotonic tensile properties: yield strength (σ_{YS}), ultimate tensile strength (σ_{UTS}), elastic modulus (E), elongation ($A80$), strain hardening exponent (n) and fracture toughness in terms of the essential work of fracture (w_e).

Direction	σ_{YS} [MPa]	σ_{UTS} [MPa]	E [GPa]	$A80$ [%]	$n_{2\text{-}20\%}$	w_e (KJ/m^2)
Transverse	567 ± 4	930 ± 2	195 ± 2	44 ± 1	0.23	347 ± 20
Longitudinal	499 ± 1	927 ± 4	180 ± 2	42 ± 1	0.25	–

Table 3
Comparison between the mean fatigue limit at 2 million cycles obtained from the standard staircase, stiffness, and self-heating methods. Fatigue limit at $R = 0.1$ (σ_e) in terms of stress amplitude, relative error (R_e) and fatigue limit to ultimate tensile strength (σ_e /σ_{UTS}) ratio.

Test	Tested specimens	σ_e [MPa]	R_e [%]	σ_e / σ_{UTS}
Staircase method	19	266 ± 23	–	0.29
Stiffness method	3	261 ± 10	−1.9	0.28
Self-heating method	3	259 ± 11	−2.5	0.28

microcracks that can propagate under fatigue. Below D_c, it is assumed that the damage is not enough to trigger fatigue crack propagation. On the contrary, high D values, typically $D \approx 1$, mean that the microcracks became a propagating macrocrack [66,67]. At this point, CDM is no longer applicable, and the crack propagation is described by LEFM. Accordingly, the evolution of D for the different stress levels has three regimes, shown in Fig. 3d: *i*) $D < D_c$, incipient damage; *ii*) $D_c \leq D \leq 1$ generation of microcracks that grow under fatigue loads and *iii*) $D \approx 1$ macrocracks growing under the LEFM framework. The σ_e is defined at the border of the regimes *i*) and *ii*), i.e., the first point where the incipient damage becomes a propagating crack. It is experimentally challenging to capture this point, so the proposed approach is to determine σ_e as the intersection point of the undamaged region ($D = 0$) and the trend shown by the small propagating cracks defined in regime *ii*) as shown in Fig. 3c. The accumulation of damage due to different loading amplitudes is not straightforward in TWIP steels, so anisotropic damage was assumed, estimating D_c as 0.5 following the work of Lemaitre et al. [51]. Additionally, experimental points at $D \approx 1$ can be used to estimate crack growth kinetics parameters.

At least three specimens were tested following this procedure. The overall testing procedure is experimentally demonstrated and discussed in the following sections.

4. Results

The monotonic mechanical properties are summarised in Table 2. They are in agreement with the values reported for similar TWIP steels with a fully austenitic microstructure [4].

Table 3 shows and compares the values of σ_e obtained by the three different testing methods. The relative error (R_e), considering the staircase value as a reference, is also given together with the σ_e / σ_{UTS} ratio. The obtained results are the same for the three methods, considering the experimental error. It is worth noticing that, if the ratio of the standard deviation of the fatigue limit to the increment of amplitude (d) is higher than 1, additional specimens should be tested, according to the recommendations of the staircase test guidelines. Representative curves for the stiffness and self-heating methods are presented in Fig. 4, showing the variation of each parameter, elongation ($\Delta\delta$) or temperature (ΔT). The elongation curve presents an exponential growth, which can be related to the generation of fatigue damage, as will be further discussed. The self-heating curve shows two regimes, as reported by Munier et al. [49]. They stated that self-heating is due to the dissipation of micro-deformation energy in different sites that are variable depending on the applied fatigue load. For low amplitudes, the active site is the elastic-plastic matrix described by the first regime. Whereas for high amplitudes, the active sites are defects, like the non-metallic inclusions, surrounded by the elastic-plastic matrix, corresponding to the second regime.

As expected, the fatigue origins are associated with the non-metallic inclusions present in the microstructure (Fig. 1). The AlN inclusions, larger than the TiN ones, act as fatigue initiation sites for all the specimens tested in the three methods (Fig. 5). According to the literature, the σ_e / σ_{UTS} ratio is higher than the expected value of 0.2. The fracture surface of the staircase specimens tested at stress levels close to the σ_e shows smooth and long fatigue fracture surfaces (Fig. 5b). On the contrary, the specimens of the stiffness method present a coarse aspect due to the high crack propagation rates (above 10^{-9} m / cycle) related to the high-stress levels applied at the tests (Fig. 5d).

5. Discussion

The two rapid fatigue methods give the same σ_e result as the staircase method. However, the time and resources needed to obtain the fatigue limit are entirely different: two weeks using a high-frequency testing machine with nineteen specimens for the standard staircase method, while only four hours and three specimens are needed with the stiffness

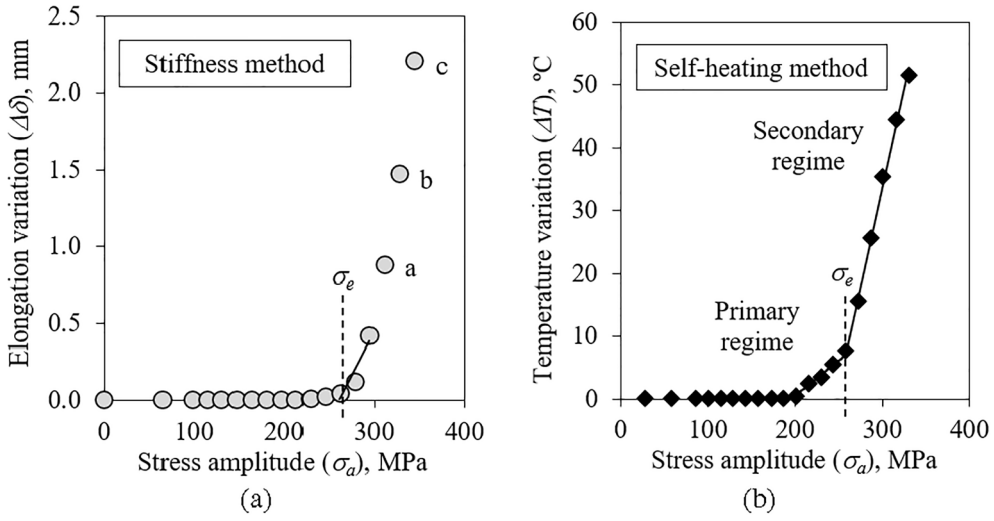

Fig. 4. A representative curve for a) stiffness method and b) self-heating method of the investigated TWIP steel. The elongation measurements labelled as a, b, c are related to Fig. 5 and Fig. 6.

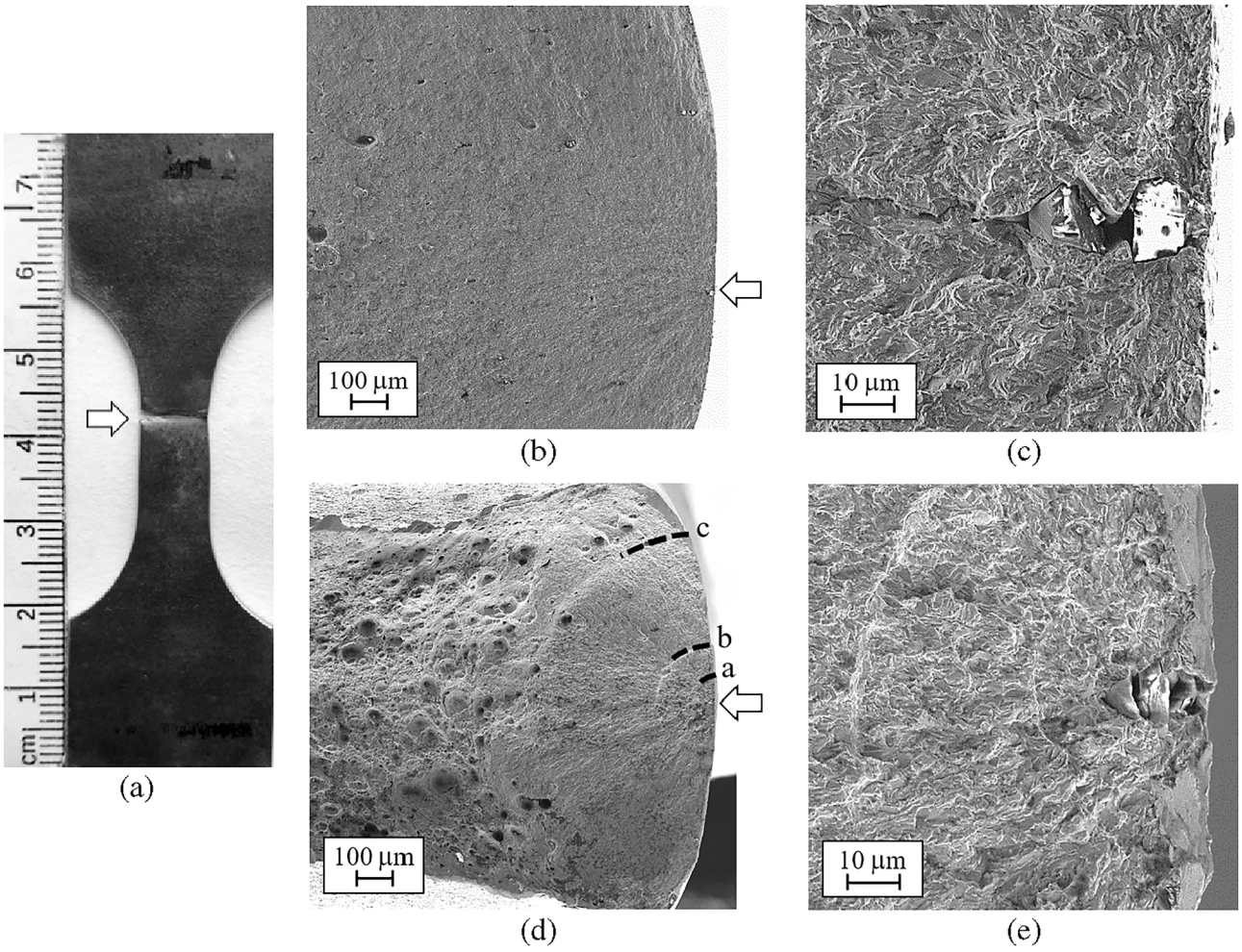

Fig. 5. a) Fractured specimen. SEM images showing the fatigue origins (white arrows) for both: b,c) staircase and d,e) stiffness method.

and the self-heating method. From an experimental point of view, the self-heating and the stiffness methods stand as interesting approaches to determine the σ_e with high accuracy in a short time and with reduced experimental resources. The good result obtained by self-heating method is shown in the literature [44,47,49], but with some drawbacks. Some authors questioned the method's accuracy when

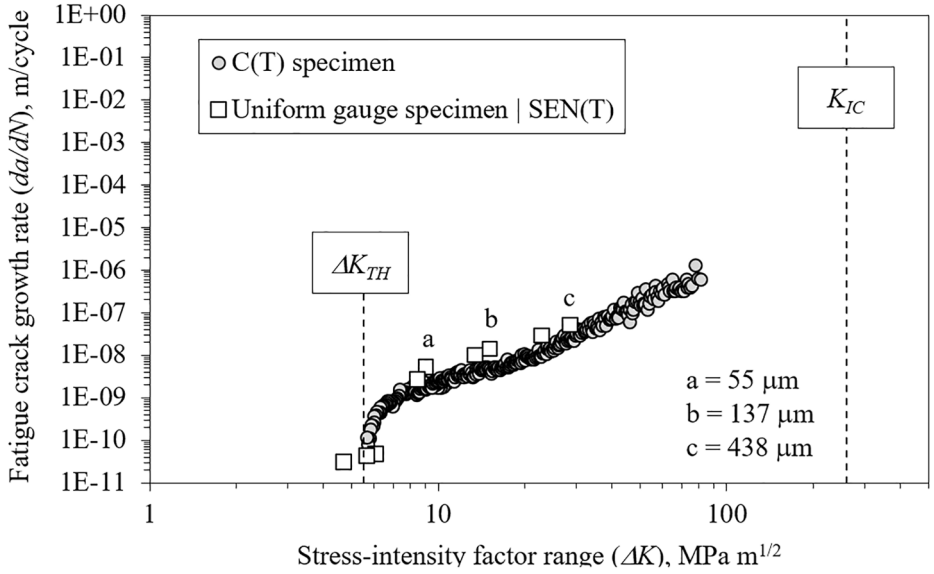

Fig. 6. FCGR of TWIP steel measured in C(T) specimens and calculated from SEN(T) specimens used in the stiffness method. The maximum K value before fracture, K_{IC} is also plotted. It is calculated from w_e and E showed in Table 2, through $K_{IC} = \sqrt{w_e E}$.

Table 4
Evaluation of the fatigue crack propagation threshold (ΔK_{TH}) calculated from Eq. (2) using experimental values of the initial fatigue defect size (a_0) and the corresponding fatigue limit (σ_e) measured in SEN(T) specimens tested using the stiffness method.

a_0 μm	σ_e [MPa]	ΔK_{TH} [MPa m$^{1/2}$]
32.9	266	6.1
21.1	258	4.7
29.9	259	5.7

Table 5
Fatigue crack propagation parameters determined in FCGR tests with C(T) specimens and the stiffness method with uniform gauge (SEN(T)) specimens. Fatigue crack propagation threshold (ΔK_{TH}) and Paris law parameters (C, m).

Specimen geometry	ΔK_{TH} [MPa m$^{1/2}$]	C[m / (cycle MPa m$^{1/2}$)]	m
C(T)	5.6	1.50×10^{-11}	2.14
SEN(T)	5.5 ± 0.7	3.12×10^{-11}	2.19

inappropriate equipment is used or to evaluate materials with a feeble self-heating effect, as in aluminium 7010 [48]. To overcome such uncertainties, other non-destructive techniques were suggested to monitor fatigue damage. For instance, Giudice et al. proposed Acoustic Emission (AE) following a similar approach to the self-heating method. The technique showed accurate results, but their experimental complexity, related to complex data processing and specific equipment handling, is a limitation [68].

The stiffness method presented in this work is developed to avoid the drawbacks and the experimental complexity of the techniques mentioned above. The method uses a state-of-the-art technique, available in many laboratories, as the DIC technique or common extensometers, which can also be easily mounted on testing machines. Moreover, the obtained data is easier to handle than the infrared cameras or the AE systems data, and the experimental procedure to determine the σ_e is more evident than in the self-heating curve.

The experimental data obtained from the stiffness method can be used to estimate the σ_e, taking the points lying in the range $0.5 \leq D \leq 1$, as well as the crack propagation behaviour of large cracks, considering points with $D \approx 1$ (Fig. 3). To verify this capability, Fig. 6 plots the FCGR obtained in C(T) specimens together with the results obtained by the stiffness method, SEN(T) specimens, showing perfect agreement in the values of ΔK_{TH} and m obtained by both approaches, as discussed below.

The ΔK_{TH} and ΔK values were estimated using Eq. (2) for the SEN(T) specimens of the stiffness method. The Y value used for these specimens was 1.13, as determined by Murakami [69]. The ΔK_{TH} was evaluated using the $\Delta\sigma$ as the measured fatigue limit and a_0 as the size of initial defects, i.e. AlN inclusions, observed in the fractographic images (Table 4). The assessed mean value for ΔK_{TH} is 5.5 ± 0.7, which perfectly matches the value measured for long cracks in FCGR tests (Table 5).

The ΔK values for the last fatigue blocks of the stiffness method belonging to the *iii*) regime were calculated using the corresponding stress range and crack size (marked with a dashed line in Fig. 5d) for SEN (T) specimens. The values labelled as *a, b, c* were plotted on the crack growth rate curve, together with the Paris curve determined in the FCGR tests (Fig. 6). Excellent agreement is found, which means that the fatigue behaviour of experimental points with a high damage level ($D \approx 1$) can be described by LEFM. Accordingly, these points associated with a macrocrack in SEN(T) specimens were used to estimate the crack propagation parameters C and m from Eq. (1). Again, a perfect agreement is found for data obtained in C(T) and SEN(T) specimens (Table 5). In addition, the obtained results are in accordance with those reported by Niendorf et al. [70] for the studied TWIP steel, showing low m exponents.

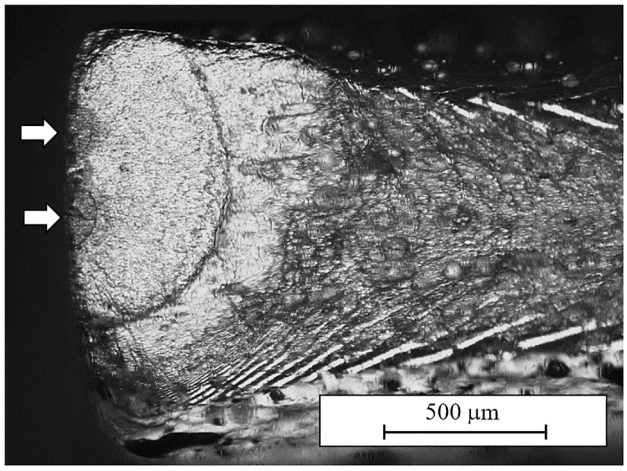

Fig. 7. Fractography of an interrupted test of the stiffness method. The crack propagation at that point was marked with Nital 2 etching. Two fatigue origins are indicated with white arrows.

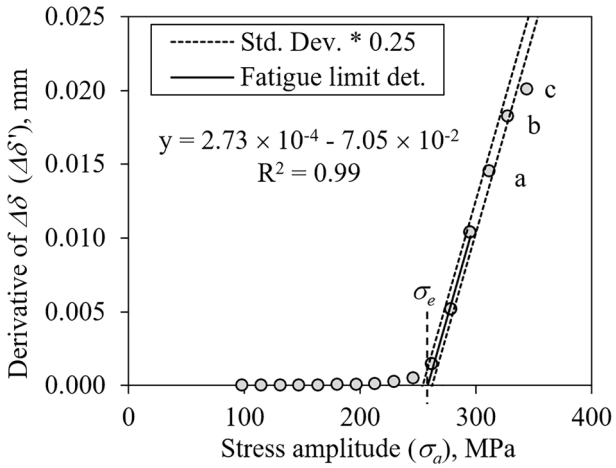

Fig. 8. A representative curve of the stiffness method using the derivative approach to select the points to determine the σ_e using data in the damage range between 0.5 and 1. The elongation measurements identified as a, b, c correspond to $D \approx 1$ and are used for LEFM calculations.

As discussed in previous works, the extrapolation of FCGR obtained with long cracks to the natural crack behaviour is always a concern [71]. The cracks studied in this work with SEN(T) specimens can be considered physically small ($a_0 < 1$ mm). However, no small crack effect is observed as the AlN inclusions that govern the fatigue nucleation are larger (28 ± 6 μm) than the austenite grain size (4.6 ± 1.2 μm) and the crack tip plasticity ($r_c = 7.5$ μm). The Eq. (6) was used to estimate the radius of the cyclic plastic zone (r_c) [72], where ΔK_I is the ΔK_{TH} and σ_Y' is the cyclic yield strength (575 MPa) reported in previous works by the authors [41]. Such similarity between FCGR between short and long crack has been shown in previous work for AHSS sheets, a press hardened steel [26].

$$r_c = \frac{1}{\pi}\left(\frac{\Delta K_I}{2\sigma_Y'}\right)^2 \tag{6}$$

Another point to be discussed is whether the D_c criterion describes well the crack nucleation and the behaviour of small cracks after its nucleation. With this aim, one test of the stiffness method was stopped when D exceeded D_c, set as 0.5 for the studied steel. The specimen was etched with Nital 2 to mark the crack shape, and then the test was continued until the final fracture. As shown in Fig. 7, small cracks of

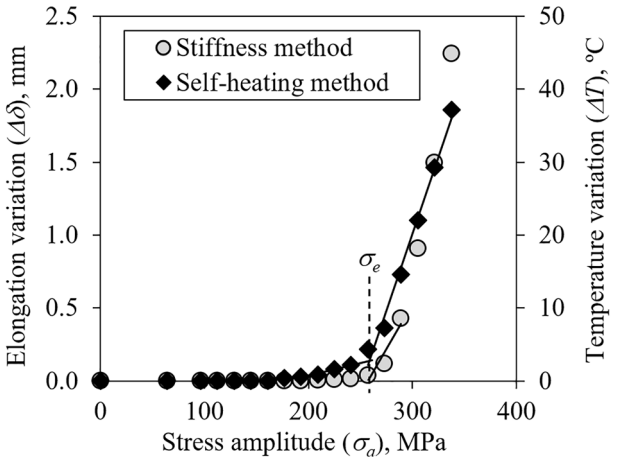

Fig. 9. Experimental fatigue curves obtained for both rapid test methods applied on a single specimen. The increment of the temperature variation can be associated with the increase in elongation related to micro and crack nucleation and propagation.

about 40 μm were detected at this damage level. It validates that microcrack nucleation is close to a damage level of 0.5, and the first propagation steps are within the damage range of $0.5 \leq D \leq 1$. Accordingly, experimental points lying in this range should be considered to estimate the σ_e and the stress level at which damage evolves into a small propagating crack would correspond to the σ_e. In order to easily determine such value, a simple approach is proposed; the derivation of the elongation variation data ($\Delta\delta'$). In this way, the transition from $D = 0$ to D_c is easily distinguished by the slope change (Fig. 8). Then, a linear fitting was done with the experimental points at the very initial crack propagation ($0.5 \leq D \leq 1$) and the intercept with the x-axis, which corresponds to zero damage and is proposed as the σ_e. Points with a deviation of larger than 25% of the standard deviation are excluded. Obtained results with three specimens following this procedure are in perfect agreement with the results obtained with the well-accepted staircase method. This good agreement confirms the hypothesis that σ_e can be estimated from D_c, as proposed by CDM. The points belonging to fracture mechanics, $D \approx 1$ with a high crack growth rate above 10^{-9} m / cycle, should be excluded for estimating σ_e and should be only considered for estimating the LEFM parameters.

Finally, both rapid test methods were carried out at the same time on a single specimen. The elongation measurements were performed on one side of the specimen and the self-heating measurements on the opposite one. The curves show that both methods predict the same σ_e (Fig. 9). Specimen damage can be calculated from the data extracted by the stiffness method and used to rationalise the temperature regimes defined in the self-heating method. The primary regime of the self-heating curve may be associated with the damage determined through D described by the CDM as the incipient fatigue damage, while the secondary regime is related to the initiation of microcracks up to the propagation of macrocracks. It is worth noticing that both rapid methods detect the damage initiation at the same stress level, either in terms of ΔT or D increase (Fig. 10). This point is named damage threshold (D_{TH}) and corresponds to the nucleation of micro-defects.

6. Summary and conclusions

This work proposes a novel method to estimate the σ_e of metal sheets, using stiffness monitoring based on CDM. The method has been successfully applied to determine the fatigue resistance of a TWIP steel, with a perfect agreement with the σ_e and the FCGR resistance obtained by well-accepted testing methods, as the staircase and the ASTM E647 procedure. According to the experimental findings, the following conclusions can be drawn:

- A rapid fatigue test method is proposed based on the measurement of the stiffness evolution. The method gives an accurate value of the fatigue limit σ_e, compared with the one obtained by the conventional staircase method, but at a concise time and with more straightforward experimental means than other rapid fatigue tests. For better accuracy, it is recommended to follow the procedure described in this work to establish the increment d and use the defined fatigue block length. Additionally, it is highly recommended to follow the considerations for the fatigue tests controlled by force determined in the ASTM E466.
- The method is rationalised by CDM; a correlation between the stiffness evolution and the different fatigue damage levels has been demonstrated. The σ_e is estimated as the stress associated with the critical damage (D_c) level when the damage generated by fatigue evolves into small propagating cracks. Such damage level has been estimated as 0.5 for the investigated TWIP steel and experimentally verified.

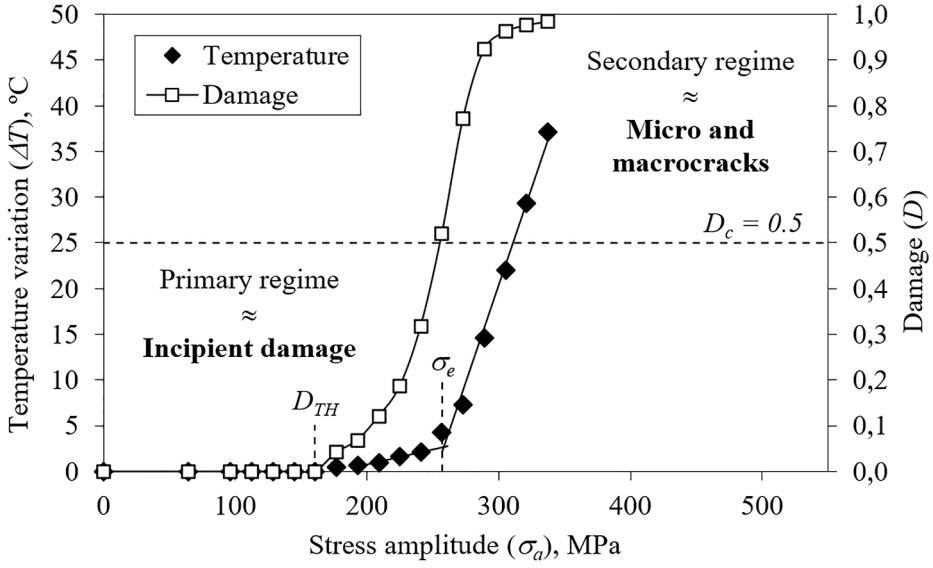

Fig. 10. Experimental fatigue curves obtained for the rapid test methods applied on a single specimen. The data for the stiffness method is represented in terms of damage and related to the different regimes of the self-heating method. Additionally, the damage threshold (D_{TH}) is plotted for both methods.

- The fatigue crack growth resistance parameters, as the Paris exponent, can be estimated from the proposed method using the points where fatigue damage is higher than 1, associated with a high crack propagation rate. The fatigue threshold ΔK_{TH}, was successfully estimated from σ_e, evaluated by the stiffness method and the size of AlN inclusions. The Paris exponent was also estimated. These fatigue parameters are in excellent agreement with values measured in C(T) specimens following standardised protocols.
- The evolution of the fatigue damage was used to rationalise the results from the self-heating method. In this case, the good relationship with the stiffness method allows associating the different regimes observed in the self-heating method with the stages of the crack development, either nucleation or propagation. Both methods also define the damage threshold D_{TH} at the same stress level.
- The presented fatigue test method allows determining the σ_e in a reduced time without using dedicated equipment such as infrared cameras or acoustic emission systems, complex experimental procedures and only using three specimens. It is presented as an easy-to-implement tool to decrease the fatigue testing time and enable faster material development, which is usually hampered by lengthy and complex fatigue tests.

Declaration of Competing Interest

The authors declare that they have no known competing financial interests or personal relationships that could have appeared to influence the work reported in this paper.

Acknowledgements

The research leading to these results has received funding from the European Union's Horizon 2020 innovation action programme under grant agreement No 101006844 – Fatigue4Light project and the Ministerio de Ciencia e Innovación (PID2019-106631GB-C41).

***Data** availability*

The raw/processed data required to reproduce these findings cannot be shared at this time due to legal or ethical reasons.

References

[1] De Cooman BC, Estrin Y, Kim SK. Twinning-induced plasticity (TWIP) steels. Acta Mater 2018;142:283–362. https://doi.org/10.1016/j.actamat.2017.06.046.
[2] Luo ZC, Liu RD, Wang X, Huang MX. The effect of deformation twins on the quasi-cleavage crack propagation in twinning-induced plasticity steels. Acta Mater 2018;150:59–68. https://doi.org/10.1016/j.actamat.2018.03.004.
[3] Chung K, Ahn K, Yoo D-H, Chung K-H, Seo M-H, Park S-H. Formability of TWIP (twinning induced plasticity) automotive sheets. Int J Plast 2011;27(1):52–81. https://doi.org/10.1016/j.ijplas.2010.03.006.
[4] Grässel O, Krüger L, Frommeyer G, Meyer LW. High strength Fe-Mn-(Al, Si) TRIP/TWIP steels development - properties - application. Int J Plast 2000;16(10-11):1391–409. https://doi.org/10.1016/S0749-6419(00)00015-2.
[5] Pierce DT, Jiménez JA, Bentley J, Raabe D, Wittig JE. The influence of stacking fault energy on the microstructural and strain-hardening evolution of Fe-Mn-Al-Si steels during tensile deformation. Acta Mater 2015;100:178–90. https://doi.org/10.1016/j.actamat.2015.08.030.
[6] Saeed-Akbari A, Imlau J, Prahl U, Bleck W. Derivation and variation in composition-dependent stacking fault energy maps based on subregular solution model in high-manganese steels. Metall Mater Trans A Phys Metall Mater Sci 2009;40(13):3076–90. https://doi.org/10.1007/s11661-009-0050-8.
[7] Martin S, Wolf S, Martin U, Krüger L. Influence of temperature on phase transformation and deformation mechanisms of cast CrMnNi-TRIP/TWIP steel. In: Solid State Phenom. Trans Tech Publications Ltd; 2011. p. 172–7. https://doi.org/10.4028/www.scientific.net/SSP.172-174.172.
[8] Shterner V, Molotnikov A, Timokhina I, Estrin Y, Beladi H. A constitutive model of the deformation behaviour of twinning induced plasticity (TWIP) steel at different temperatures. Mater Sci Eng A 2014;613:224–31. https://doi.org/10.1016/j.msea.2014.06.073.
[9] Sato K, Ichinose M, Hirotsu Y, Inoue Y. Effects of Deformation Induced Phase Transformation and Twinning on the Mechanical Properties of Austenitic Fe-Mn-AI Alloys. Isij Int 1989;29:868–77. https://doi.org/10.2355/isijinternational.29.868.
[10] Sabzi HE, Zarei-Hanzaki A, Abedi HR, Mateo A, Roa JJ. The sequential twinning-transformation induced plasticity effects in a thermomechanically processed high Mn austenitic steel. Mater Sci Eng A 2018;725:242–9. https://doi.org/10.1016/j.msea.2018.03.102.
[11] Ishida K, Nishizawa T. Effect of alloying elements on stability of epsilon iron. Trans Jap Inst Met 1974;15(3):225–31. https://doi.org/10.2320/matertrans1960.15.225.
[12] Bouaziz O, Guelton N. Modelling of TWIP effect on work-hardening. Mater Sci Eng A 2001;319–321:246–9. https://doi.org/10.1016/S0921-5093(00)02019-0.
[13] Frómeta D, Lara A, Molas S, Casellas D, Rehrl J, Suppan C, et al. On the correlation between fracture toughness and crash resistance of advanced high strength steels. Eng Fract Mech 2019;205:319–32. https://doi.org/10.1016/j.engfracmech.2018.10.005.
[14] Frommeyer G, Brüx U, Neumann P. Supra-ductile and high-strength manganese-TRIP/TWIP steels for high energy absorption purposes. ISIJ Int 2003;43(3):438–46. https://doi.org/10.2355/isijinternational.43.438.
[15] Madivala M, Bleck W. Strain Rate Dependent Mechanical Properties of TWIP Steel. JOM 2019;71(4):1291–302. https://doi.org/10.1007/s11837-018-3137-0.
[16] Shao CW, Zhang P, Zhu YK, Zhang ZJ, Pang JC, Zhang ZF. Improvement of low-cycle fatigue resistance in TWIP steel by regulating the grain size and distribution. Acta Mater 2017;134:128–42. https://doi.org/10.1016/j.actamat.2017.05.004.
[17] Cornette D, Cugy P, Hildenbrand A, Bouzekri M, Lovato G. Aciers à très haute résistance FeMn TWIP pour pièces de sécurité dans la construction automobile. Rev Metall Cah D'Informations Tech 2005;102:905–18. https://doi.org/10.1051/metal:2005151.
[18] Fleck NA, Kang KJ, Ashby MF. Overview no. 112. The cyclic properties of engineering materials. Acta Metall Mater 1994;42:365–81. https://doi.org/10.1016/0956-7151(94)90493-6.
[19] Hamada AS, Karjalainen LP, Ferraiuolo A, Gil Sevillano J, De Las Cuevas F, Pratolongo G, et al. Fatigue behavior of four high-Mn twinning induced plasticity effect steels. In. Metall Mater Trans A Phys Metall Mater Sci. Springer 2010:1102–8. https://doi.org/10.1007/s11661-010-0193-7.
[20] Karjalainen LP, Hamada A, Misra RDK, Porter DA. Some aspects of the cyclic behavior of twinning-induced plasticity steels. Scr Mater 2012;66(12):1034–9. https://doi.org/10.1016/j.scriptamat.2011.12.008.
[21] Roa JJ, Fargas G, Calvo J, Jiménez-Piqué E, Mateo A. Plastic deformation and damage induced by fatigue in TWIP steels. Mater Sci Eng A 2015;628:410–8. https://doi.org/10.1016/j.msea.2015.01.043.
[22] Seo W, Jeong D, Sung H, Kim S. Tensile and high cycle fatigue behaviors of high-Mn steels at 298 and 110 K. Mater Charact 2017;124:65–72. https://doi.org/10.1016/j.matchar.2016.12.001.
[23] Gui LM, Jin XC, Li HT, Zhang M. High cycle fatigue performances of advanced high strength steel CP800. Adv Mater Res, Trans Tech Publications Ltd 2014:238–41. https://doi.org/10.4028/www.scientific.net/AMR.989-994.238.
[24] Lara A, Picas I, Casellas D. Effect of the cutting process on the fatigue behaviour of press hardened and high strength dual phase steels. J Mater Process Technol 2013;213(11):1908–19. https://doi.org/10.1016/j.jmatprotec.2013.05.003.
[25] Mohammad KA, Zainudin ES, Sapuan S, Zahari NI, Ali A. Fatigue life for type 316L stainless steel under cyclic loading. In: Adv Mater Res. Trans Tech Publications Ltd; 2013. p. 77–81. https://doi.org/10.4028/www.scientific.net/AMR.701.77.
[26] Parareda S, Casellas D, Frómeta D, Martínez M, Lara A, Barrero A, et al. Fatigue resistance of press hardened 22MnB5 steels. Int J Fatigue 2020;130:105262. https://doi.org/10.1016/j.ijfatigue.2019.105262.
[27] Wang B, Zhang ZJ, Shao CW, Duan QQ, Pang JC, Yang HJ, et al. Improving the High-Cycle Fatigue Lives of Fe-30Mn-0.9C Twinning-Induced Plasticity Steel Through Pre-straining. Metall Mater Trans A Phys Metall Mater Sci 2015;46(8):3317–23. https://doi.org/10.1007/s11661-015-3010-5.
[28] Wang B, Zhang P, Duan QQ, Zhang ZJ, Yang HJ, Pang JC, et al. High-cycle fatigue properties and damage mechanisms of pre-strained Fe-30Mn-0.9C twinning-induced plasticity steel. Mater Sci Eng A 2017;679:258–71. https://doi.org/10.1016/j.msea.2016.10.043.
[29] Song SW, Lee JH, Lee HJ, Bae CM, Lee CS. Enhancing high-cycle fatigue properties of cold-drawn Fe-Mn-C TWIP steels. Int J Fatigue 2016;85:57–64. https://doi.org/10.1016/j.ijfatigue.2015.12.007.
[30] Kim YW, Kim G, Hong S-G, Lee CS. Energy-based approach to predict the fatigue life behavior of pre-strained Fe-18Mn TWIP steel. Mater Sci Eng A 2011;528(13-14):4696–702. https://doi.org/10.1016/j.msea.2011.02.068.
[31] Wang B, Zhang P, Duan QQ, Zhang ZJ, Yang HJ, Pang JC, et al. Synchronously improved fatigue strength and fatigue crack growth resistance in twinning-induced plasticity steels. Mater Sci Eng A 2018;711:533–42. https://doi.org/10.1016/j.msea.2017.11.074.
[32] Niendorf T, Lotze C, Canadinc D, Frehn A, Maier HJ. The role of monotonic pre-deformation on the fatigue performance of a high-manganese austenitic TWIP steel. Mater Sci Eng A 2009;499(1-2):518–24. https://doi.org/10.1016/j.msea.2008.09.033.
[33] Rüsing CJ, Lambers H-G, Lackmann J, Frehn A, Nagel M, Schaper M, et al. Property Optimization for TWIP Steels - Effect of Pre-deformation Temperature on Fatigue Properties. Mater Today Proc, Elsevier Ltd 2015;2:S681–5. https://doi.org/10.1016/j.matpr.2015.07.375.
[34] Shao CW, Zhang P, Wang XG, Wang Q, Zhang ZF. High-cycle fatigue behavior of TWIP steel with graded grains: breaking the rule of mixture. Mater Res Lett 2019;7(1):26–32. https://doi.org/10.1080/21663831.2018.1550822.
[35] Hamada AS, Karjalainen LP. High-cycle fatigue behavior of ultrafine-grained austenitic stainless and TWIP steels. Mater Sci Eng A 2010;527(21-22):5715–22. https://doi.org/10.1016/j.msea.2010.05.035.

[36] Sen I, Tamirisakandala S, Miracle D, Ramamurty U. Microstructural effects on the mechanical behavior of B-modified Ti-6Al-4V alloys. Acta Mater 2007;55(15):4983–93. https://doi.org/10.1016/j.actamat.2007.05.009.
[37] Nikulin I, Sawaguchi T, Tsuzaki K. Effect of alloying composition on low-cycle fatigue properties and microstructure of Fe-30Mn-(6–x)Si-xAl TRIP/TWIP alloys. Mater Sci Eng A 2013;587:192–200. https://doi.org/10.1016/j.msea.2013.08.061.
[38] Glage A, Weidner A, Biermann H. Cyclic deformation behaviour of three austenitic cast CrMnNi TRIP/TWIP steels with various Ni content. Steel Res Int 2011;82(9):1040–7. https://doi.org/10.1002/srin.201100080.
[39] Klein MW, Blinn B, Smaga M, Beck T. High cycle fatigue behavior of high-Mn TWIP steel with different surface morphologies. Int J Fatigue 2020;134:105499. https://doi.org/10.1016/j.ijfatigue.2020.105499.
[40] Klein MW, Smaga M, Beck T. Surface morphology and its influence on cyclic deformation behavior of high-Mn TWIP steel. Metals (Basel) 2018;8:832. https://doi.org/10.3390/met8100832.
[41] Lara A, Roca M, Parareda S, Cuadrado N, Calvo J, Casellas D, et al. Effect of Sandblasting on Low and High-Cycle Fatigue Behaviour after Mechanical Cutting of a Twinning-Induced Plasticity Steel. MATEC Web Conf 2018;165:18002. https://doi.org/10.1051/matecconf/201816518002.
[42] Stromeyer CE. The determination of fatigue limits under alternating stress conditions. Proc R Soc London. Ser A, Contain Pap a Math Phys Character 1914;90:411–25. https://doi.org/10.1098/rspa.1914.0066.
[43] Luong MP. Fatigue limit evaluation of metals using an infrared thermographic technique. Mech Mater 1998;28(1-4):155–63. https://doi.org/10.1016/S0167-6636(97)00047-1.
[44] La Rosa G, Risitano A. Thermographic methodology for rapid determination of the fatigue limit of materials and mechanical components. Int J Fatigue 2000;22:65–73. https://doi.org/10.1016/S0142-1123(99)00088-2.
[45] Fargione G, Geraci A, La Rosa G, Risitano A. Rapid determination of the fatigue curve by the thermographic method. Int J Fatigue 2002;24:11–9. https://doi.org/10.1016/S0142-1123(01)00107-4.
[46] Amiri M, Khonsari MM. Rapid determination of fatigue failure based on temperature evolution: Fully reversed bending load. Int J Fatigue 2010;32(2):382–9. https://doi.org/10.1016/j.ijfatigue.2009.07.015.
[47] Ricotta M, Meneghetti G, Atzori B, Risitano G, Risitano A. Comparison of experimental thermal methods for the fatigue limit evaluation of a stainless steel. Metals (Basel) 2019;9(6):677. https://doi.org/10.3390/met9060677.
[48] Krapez J-C, Pacou D, Gardette G. Lock-in thermography and fatigue limit of metals. in 2000. https://doi.org/10.21611/qirt.2000.051.
[49] Munier R, Doudard C, Calloch S, Weber B. Determination of high cycle fatigue properties of a wide range of steel sheet grades from self-heating measurements. Int J Fatigue 2014;63:46–61. https://doi.org/10.1016/j.ijfatigue.2014.01.004.
[50] MENEGHETTI G. Analysis of the fatigue strength of a stainless steel based on the energy dissipation. Int J Fatigue 2007;29(1):81–94. https://doi.org/10.1016/j.ijfatigue.2006.02.043.
[51] Lemaitre J, Desmorat R. Engineering damage mechanics: Ductile, creep, fatigue and brittle failures. Eng Damage Mech Ductile, Creep, Fatigue Brittle Fail 2005:1–380. https://doi.org/10.1007/B138882.
[52] Barbu LG, Oller S, Martinez X, Barbat A. High cycle fatigue simulation: A new stepwise load-advancing strategy. Eng Struct 2015;97:118–29. https://doi.org/10.1016/J.ENGSTRUCT.2015.04.012.
[53] Liu N, Cui X, Xiao J, Lua J, Phan N. A simplified continuum damage mechanics based modeling strategy for cumulative fatigue damage assessment of metallic bolted joints. Int J Fatigue 2020;131:105302. https://doi.org/10.1016/j.ijfatigue.2019.105302.
[54] Oller S, Salomón O, Oñate E. A continuum mechanics model for mechanical fatigue analysis. Comput Mater Sci 2005;32(2):175–95. https://doi.org/10.1016/j.commatsci.2004.08.001.
[55] Zhan Z, Hu W, Li B, Zhang Y, Meng Q, Guan Z. Continuum damage mechanics combined with the extended finite element method for the total life prediction of a metallic component. Int J Mech Sci 2017;124–125:48–58. https://doi.org/10.1016/J.IJMECSCI.2017.03.002.
[56] Grosskreutz JC. Strengthening and Fracture in Fatigue (Approaches for achieving high fatigue strength). Met Trans 1972;3(5):1255–62. https://doi.org/10.1007/BF02642460.
[57] Bouaziz O, Allain S, Scott CP, Cugy P, Barbier D. High manganese austenitic twinning induced plasticity steels: A review of the microstructure properties relationships. Curr Opin Solid State Mater Sci 2011;15(4):141–68. https://doi.org/10.1016/j.cossms.2011.04.002.
[58] Hong S, Shin SY, Kim HS, Lee S, Kim S-K, Chin K-G, et al. Effects of inclusions on delayed fracture properties of three twinning induced plasticity (TWIP) steels. Metall Mater Trans A Phys Metall Mater Sci 2013;44(2):776–86. https://doi.org/10.1007/s11661-012-1472-2.
[59] Xu Le, Barlat F, Lee M-G. Hole expansion of twinning-induced plasticity steel. Scr Mater 2012;66(12):1012–7. https://doi.org/10.1016/j.scriptamat.2012.01.062.
[60] Kusakin P, Belyakov A, Kaibyshev R, Molodov D. Effect of Cold Rolling on Microstructure and Mechanical Properties of a Fe-23Mn-0.3C-1.5Al TWIP Steel; n. d. doi: 10.4028/www.scientific.net/AMR.922.394.
[61] Einbock S. Statistics of Metal Fatigue in Engineering: Planning and Analysis of Metal Fatigue Tests. 3rd ed. Books on Demand; 2018.
[62] ASTM E466. Standard Practice for Conducting Force Controlled Constant Amplitude Axial Fatigue Tests of Metallic Materials. American Society for Testing and Materials; 1996.
[63] ASTM E647. Standard Test Method for Measurement of Fatigue Crack Growth Rates. American Society for Testing and Materials; 2000.
[64] ASTM E1823. Standard Terminology Relating to Fatigue and Fracture Testing. American Society for Testing and Materials; 2013.
[65] Kachanov LM. Time of the Rupture Process under Creep Conditions, Izy Akad, 8. Otd Tech Nauk; 1958. p. 26–31.
[66] Murakami S. In: Continuum Damage Mechanics: A Continuum Mechanics Approach to the Analysis of Damage and Fracture. Netherlands: Springer; 2012. https://doi.org/10.1007/978-94-007-2666-6.
[67] Chaboche JL. Continuum damage mechanics: Part I-general concepts. J Appl Mech Trans ASME 1988;55:59–64. https://doi.org/10.1115/1.3173661.
[68] Giudice F, La Rosa G, Lo Savio F, Clienti C. Comparison between thermal energy and acoustic emission for the fatigue behavior of steels. Procedia Struct Integr 2019;18:886–90. https://doi.org/10.1016/j.prostr.2019.08.239.
[69] Murakami Y, Keer LM. Stress Intensity Factors Handbook. J Appl Mech 1993;360:1063. https://doi.org/10.1115/1.2900983.
[70] Niendorf T, Rubitschek F, Maier HJ, Niendorf J, Richard HA, Frehn A. Fatigue crack growth-Microstructure relationships in a high-manganese austenitic TWIP steel. Mater Sci Eng A 2010;527(9):2412–7. https://doi.org/10.1016/j.msea.2009.12.012.
[71] Chapetti M. Fatigue propagation threshold of short cracks under constant amplitude loading. Int J Fatigue 2003;25(12):1319–26. https://doi.org/10.1016/S0142-1123(03)00065-3.
[72] Suresh S. Fatigue of Materials. 2nd ed. Cambridge: Cambridge University Press; 1998. https://doi.org/10.1017/cbo9780511806575.